Synthesis and Characterization of a Novel Covalently Functionalized Organoclay and Its Polypropylene Nanocomposite

Xiaohua Du,[1,2] Zhenjiang Zhang,[1,2] Haiou Yu,[1,2] Dong Wan,[1,2] Haiping Xing,[1,2] Tao Tang[1]

[1]*State Key Laboratory of Polymer Physics and Chemistry, Changchun Institute of Applied Chemistry, Chinese Academy of Sciences, Changchun 130022, China*
[2]*Graduate School of the Chinese Academy of Sciences, Beijing 100039, China*

Received 28 April 2009; accepted 18 July 2009
DOI 10.1002/app.31143
Published online 15 September 2009 in Wiley InterScience (www.interscience.wiley.com).

ABSTRACT: A covalently functionalized organoclay was synthesized successfully through a condensation reaction of SiOH groups on the edge of montmorillonite (MMT) with acryloyl chloride followed by modification with hexadecyltrimethylammonium bromide (CTAB) via an ion-exchange reaction. Fourier transform infrared confirmed that C=C groups had been grafted to MMT sheets. Wide-angle X-ray diffraction measurements showed that CTAB had intercalated into MMT interlayers. The content of bonded acryloyl chloride was 2.42 wt % in the functionalized organoclay according to thermogravimetric analysis. Polypropylene (PP) nanocomposites were prepared by melt mixing. Rheological measurements and morphology observations confirmed that PP nanocomposites containing the organoclay bearing C=C groups exhibited improved interfacial interaction between PP chains and MMT sheets. Thus, the PP nanocomposites showed not only higher storage modulus and complex viscosity values at low frequencies but also enhanced mechanical properties. © 2009 Wiley Periodicals, Inc. J Appl Polym Sci 115: 1105–1112, 2010

Key words: clay; interfaces; nanocomposites; poly(propylene) (PP)

INTRODUCTION

In recent years, polymer–clay nanocomposites have attracted much attention in both academia and industry because they often exhibit great improvements in mechanical properties, thermal stability, flame retardance, and barrier properties with only small amounts of clay.[1–3] The most common strategies for preparing polymer–clay nanocomposites fall into three categories: *in situ* polymerization, solution blending, and melt mixing. Melt mixing is considered to be a preferable method for industrial manufacturing because of the absence of a solvent and the short processing time. Before melt mixing, the key step is to make a hydrophilic clay more hydrophobic by the modification of the clay with an alkylammonium surfactant via an ion-exchange reaction. This will increase the interlayer distance of the clay and improve the miscibility between the polymer and clay. Of course, a compatibilizer is often added to improve the compatibility and increase the dispersion of the clay in the polymer matrix. Besides the dispersion degree of the clay, the increased performance is also dependent on the interaction between the polymer and clay.[4–6]

Isomorphic substitution within montmorillonite (MMT) sheets (e.g., Al^{3+} replaced by Mg^{2+} or Fe^{2+}) generates negative charges that are counterbalanced by Na^{+} or Ca^{2+} ions in the interlayer, which induce MMT's cation-exchange capacity. On the other hand, there are some SiOH groups on the edges of MMT sheets, so MMT can be chemically modified. Recently, covalent reactions of chloro or alkoxy silanes with edge SiOH groups have been reported, and silane coupling agents have been covalently grafted to MMT sheets.[7–9] If MMT sheets are modified by a silane coupling agent possessing functional groups, polymer chains will be grafted to MMT layers through later *in situ* polymerization of the monomer with the functional groups.[10]

High-melt-strength polypropylene (PP) is often prepared by the reactive extrusion of PP with peroxide and a multifunctional monomer.[11–13] Because of the chemical nature of PP, it has a tendency to undergo β scission during melt processing. The fragmental free radical could react with the

Correspondence to: T. Tang (ttang@ciac.jl.cn).
Contract grant sponsor: National Natural Science Foundation of China; contract grant numbers: 50525311 (for an outstanding youth project), 50873099 (for a general project).
Contract grant sponsor: Fund for Creative Research Groups; contract grant number: 50621302.

TABLE I
Compositions of the PP Nanocomposites

Sample	PP (wt %)	PPMA1001 (wt %)	F-organoclay (wt %)	CTAB-modified MMT (wt %)
PP0	100	0	0	0
PP1	96	3	1	0
PP2	88	9	3	0
PP3	80	15	5	0
PP4	68	24	8	0
PP5	80	15	0	5
PP6	80	15	0	0

multifunctional monomer and introduce a long-chain-branched structure and even a crosslinked structure into the polymer matrix. Could the fragmental free radical produced from the degradation of PP in melt mixing be used to improve the interfacial interaction between PP and MMT?

With this in mind, we synthesized a novel organoclay in this work. We first grafted C=C groups to MMT layers by reacting the edge SiOH groups with acryloyl chloride. Then, the functionalized MMT was modified with hexadecyltrimethylammonium bromide (CTAB) through an ion-exchange reaction. Furthermore, the functionalized organoclay (F-organoclay) was used as a multifunctional monomer to melt-mix with the PP resin. The resultant PP nanocomposites were characterized.

EXPERIMENTAL

Materials

The MMT used in this study was supplied by Kunimine Co., Ltd. (Tokyo, Japan) with a cation-exchange capacity of 119 mequiv/100 g. CTAB was purchased from Shanghai Huishi Chemical Co., Ltd. (Shanghai, China). Acryloyl chloride (96% purity) was obtained from Alfa Aesar. Chloroform (analytical reagent) and ethanol (analytical reagent) were purchased from Beijing Chemical Works (Beijing, China). PP (F401) was purchased from Panjin Petrochemical with a melt flow index of 0.8 g/min. Maleic anhydride grafted polypropylene (PPMA1001; acid value = 26 mg of KOH/g) was purchased from Sanyo Chemical Industries.

Synthesis of the F-organoclay

MMT was first dried in a vacuum oven at 80°C for 48 h. The predried MMT was stirred in chloroform for 3 h, and then acryloyl chloride was added. The mixture was stirred at room temperature for 10 h before it was heated to 65°C and refluxed for 6 h. After cooling, the product was filtered and washed with ethanol and then was dried in a vacuum oven at 60°C for 12 h. Several droplets of pyridine were added to the system as an absorber. The acryloyl chloride treated montmorillonite (A-MT) was further surface-modified by CTAB via an ion-exchange reaction as follows. A-MT was first dispersed in deionized water, then a CTAB solution in deionized water was added, and the mixture was stirred strongly overnight. The amount of CTAB agreed with a 100% cation-exchange capacity of MMT. The obtained F-organoclay was filtered and washed with hot deionized water. Finally, the product was dried in a vacuum oven at 60°C for 24 h and then ground in a mortar for further use.

Preparation of the PP/clay nanocomposites

The PP/clay nanocomposites were fabricated through the melt blending of PP, PPMA1001, and modified MMTs in a Brabender (Shanghai, China) mixer with a rotating speed of 100 rpm at 180°C for 10 min. The ratio of the compatibilizer (PPMA1001) to the clay was 3:1 by weight. The samples were transferred to a mold and preheated at 180°C and then were pressed to obtain 1-mm-thick plates for characterization. Pure PP and a PP/PPMA1001 blend were also melt-mixed as a control. The compositions of the samples are listed in Table I.

Characterization

Wide-angle X-ray diffraction (WAXD) was carried out on a Rigaku (Tokyo, Japan) model D/max 2500 with Cu Kα radiation, and the interlayer distances (d_{001}) of the samples were estimated from the (001) peaks in the WAXD patterns with the Bragg formula. The X-ray generator was operated at a voltage of 40 kV and 200 mA. With a Bruker Vertex 70 Fourier transform infrared (FTIR) spectrometer, FTIR spectra of the organoclays were collected at room temperature. Thermogravimetric analysis (TGA) was performed under a nitrogen flow from room temperature to 800°C at a heating rate of 10°C min^{-1} with a TA Instruments SDT Q600. Transmission electron microscopy (TEM) images of PP nanocomposites were taken with a transmission electron microscope (JEM1011, JEOL) operated at an accelerating voltage of 100 kV without staining. The specimens were sectioned into 80-nm thin films at −90°C in a Leica

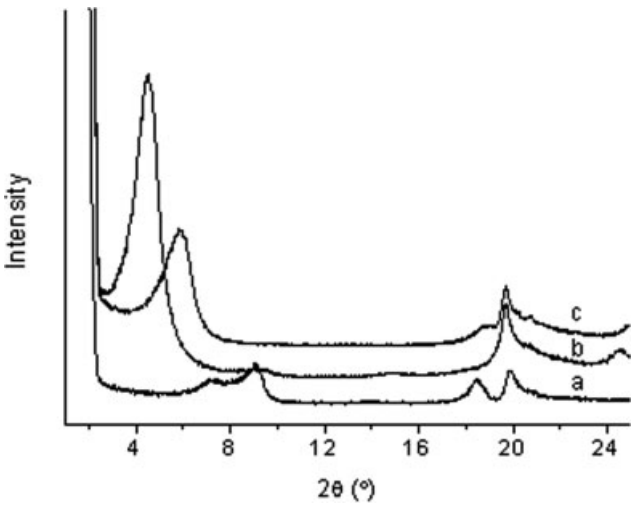

Figure 1 WAXD patterns of (a) MMT, (b) the organoclay synthesized through the modification of MMT with CTAB, and (c) the sample prepared by the treatment of CTAB-modified MMT with acryloyl chloride.

Ultracut R with FCS. PP nanocomposites were packed with filter paper and then extracted in a Soxhlet extractor with boiling xylene for 24 h. The residue was dried *in vacuo*. The morphologies of the residue were observed with a Philips XL-30 environmental scanning electron microscope (SEM, Netherlands). The rheological properties were determined on a Reologica Stresstech with a parallel-plate geometry 20 mm in diameter. The oscillatory measurements were carried out with a gap distance of 0.8 mm and a controlled strain of 1%. The complex viscosity (η^*) and storage modulus (G') were measured as functions of the angular frequency (ranging from 0.03 to 100 rad/s) at 180°C in a nitrogen atmosphere. The static mechanical properties were measured with an Instron 1121 tensile testing machine, and the crosshead rate was fixed at 50 mm/min. For each data point, five samples were tested, and the average value was taken.

RESULTS AND DISCUSSION

Synthesis and characterization of the F-organoclay

Two different routes were attempted to synthesize the F-organoclay bearing C=C groups. First, MMT was surface-modified with CTAB via an ion-exchange reaction before it reacted with acryloyl chloride. Figure 1 shows the WAXD patterns of the obtained organoclays. The (001) diffraction peak of the CTAB-modified MMT [Fig. 1(b)] was located at a lower angle with respect to that of the original MMT [Fig. 1(a)]. This means that CTAB intercalated into the interlayers of MMT. After the CTAB-modified MMT further reacted with acryloyl chloride, the (001) diffraction peak of the resultant F-organoclay shifted to a higher degree [$2\theta = 5.9°$; Fig. 1(c)] in comparison with that of the CTAB-modified MMT. We concluded that the latter reaction decreased the interlayer distance of the F-organoclay. Because acryloyl chloride reacted with the CTAB-modified MMT with chloroform as the solvent, some of the intercalated CTAB was dissolved in chloroform and washed out. Therefore, the interlayer distance of the F-organoclay decreased.[14]

In the second route, MMT first reacted with acryloyl chloride (named A-MT), and this was followed by surface modification with CTAB. The process for modifying MMT through this route is revealed in Scheme 1. The WAXD patterns of the samples are displayed in Figure 2. The weak peak at $2\theta = 7.2°$ in the original MMT resulted from absorbed water in the gallery of MMT [Fig. 2(a)]. The WAXD pattern of A-MT showed the main diffraction peak at $2\theta = 7.1°$ [Fig. 2(b)], which was lower than that of the original MMT ($2\theta = 9.1°$). Pyridine was used as an absorber for the produced acid. After pyridine was protonated, it could intercalate into the interlayers of MMT by an ion-exchange reaction and slightly increased the interlayer distance. A-MT was further modified by CTAB via an ion-exchange reaction. As shown in Figure 2(c), the (001) diffraction peak of the resultant F-organoclay was at $2\theta = 4.68°$ with an interlayer distance of 1.9 nm.

According to these results, the obtained F-organoclay prepared by the second route possessed a larger interlayer distance in comparison with those from the first route. Figure 3 displays FTIR spectra of the F-organoclay obtained by the second route. The peak at 1638 cm^{-1} in Figure 3(a) is due to the OH bending vibration of the absorbed water on the surface of MMT.[15] The stretching vibration of C=C belonging to acryloyl chloride is overlapped by the OH

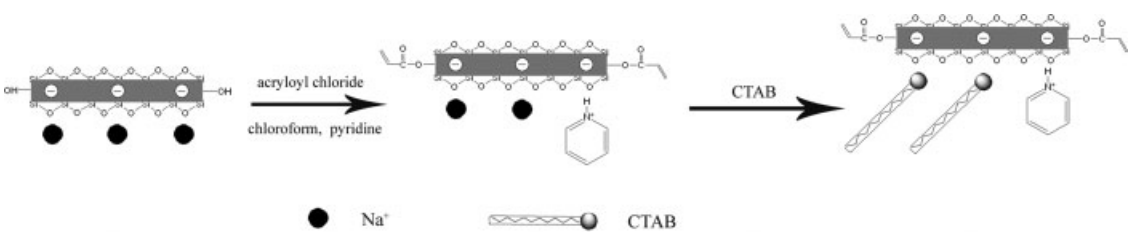

Scheme 1 Schematic drawing of the modification of MMT by the second route.

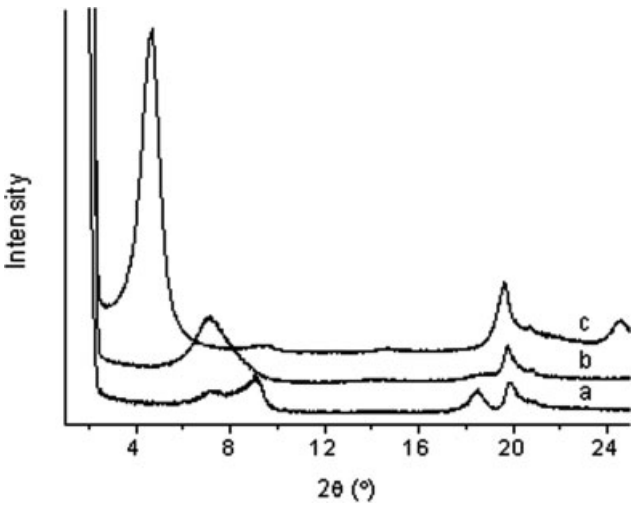

Figure 2 WAXD patterns of (a) MMT, (b) A-MT, and (c) the sample prepared through the modification of A-MT with CTAB via an ion-exchange reaction.

bending vibration in Figure 3(b,c). However, the peak at 1732 cm^{-1} in Figure 3(b,c) corresponds to the C=O stretching vibration of acryloyl chloride, and this indicates that acryloyl chloride reacted with the SiOH group on the edge of MMT and bonded to MMT layers. The peaks at 2926, 2852, and 1473 cm^{-1} for the CH_2 asymmetric stretching vibration, symmetric stretching vibration, and bending vibration, respectively, can be observed in Figure 3(c), supporting the intercalation of CTAB into the interlayers of A-MT.

TGA was used to evaluate the amount of C=C groups in the F-organoclays. Figure 4 shows TGA curves of the F-organoclay obtained with the second route. As is known, protonated pyridine can embed into MMT layers, and this decreases the amount of CTAB intercalated into MMT layers. In comparison with MMT, the mass loss of A-MT was 3.99%, including bonded acryloyl chloride and protonated pyridine. The CTAB-modified MMT had a mass loss of 27.18%. CTAB-modified A-MT (F-organoclay) had a mass loss of 24.02%. The difference in the mass loss between the CTAB-modified MMT and F-organoclay resulted from some CTAB being replaced by protonated pyridine and edge-bonded acryloyl chloride. The content of covalently bonded acryloyl chloride could be calculated with the followed equation:

$$\frac{27.18 - (24.02 - 3.99)}{M_c} = \frac{3.99 - x}{M_p}$$

where M_c is the molecular weight of CTAB (364), M_p is the molecular weight of protonated pyridine (80), and x is the amount of bonded acryloyl chloride. The result shows $x = 2.42\%$; this means that 2.42 g of acryloyl chloride was bonded to 100 g of the F-organoclay. The amount of C=C groups was 0.044 mol/100 g of the F-organoclay.

Rheological behavior of the PP/F-organoclay nanocomposites

Compared to pure polymers, polymer–clay nanocomposites often show higher G' and η^* values at low frequencies, and this is explained by the existence of a percolated network microstructure.[16–19] As shown in Figure 5(a,b), the G' and η^* values of the PP nanocomposite (PP5) increased in the low frequency region when CTAB-modified MMT was added to PP. However, after the F-organoclay was added to PP (PP3), the obtained nanocomposite had higher G' and η^* values than PP5 at low frequencies.

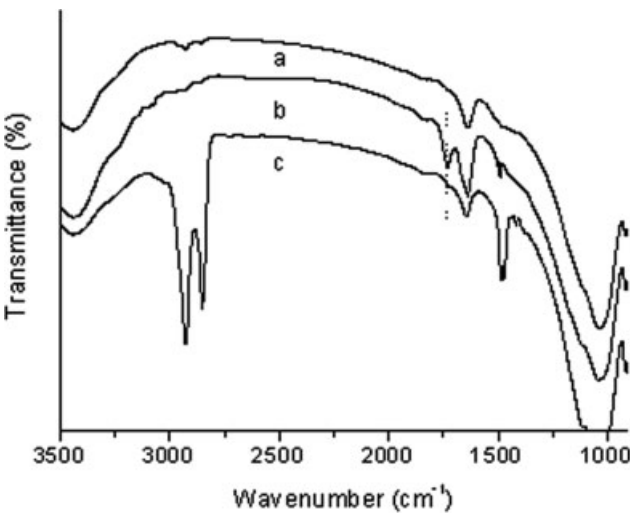

Figure 3 FTIR spectra of (a) MMT, (b) A-MT, and (c) the sample prepared through the modification of A-MT with CTAB via an ion-exchange reaction.

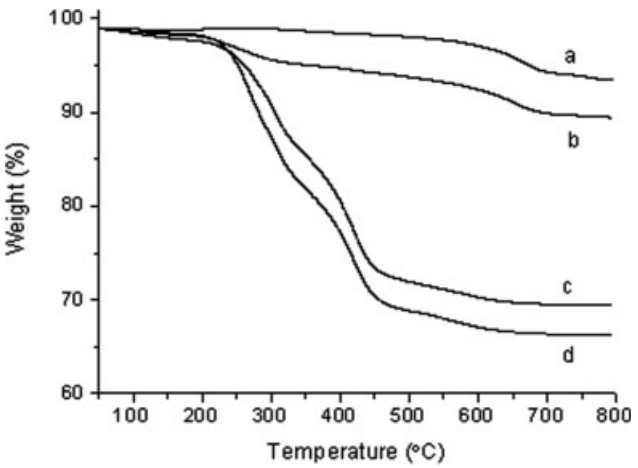

Figure 4 TGA curves of (a) MMT, (b) A-MT, (c) the sample prepared through the modification of A-MT with CTAB via an ion-exchange reaction, and (d) the organoclay synthesized through the modification of MMT with CTAB.

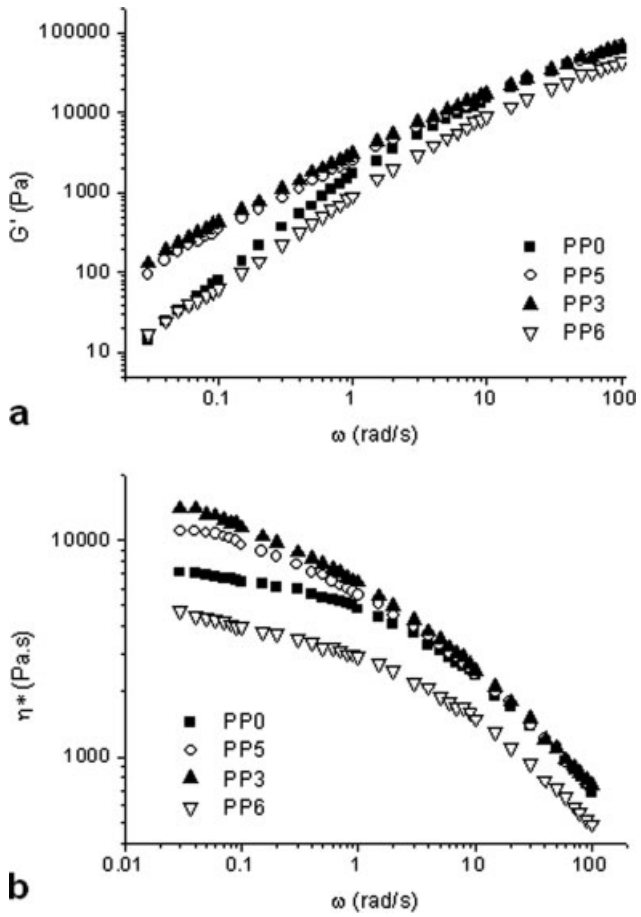

Figure 5 (a) G' and (b) η^* as functions of the angular frequency (ω) for PP0, PP5, PP3, and PP6.

The effect of the compatibilizer (PPMA1001) on the rheological properties of PP was also investigated. In PP6, the addition of PPMA1001 did not obviously change G' in the absence of modified MMTs at low frequencies but reduced η^* at all frequencies because of an effect of dilution of PPMA1001.[18] This further confirms that the increases in G' and η^* of the PP nanocomposites, in comparison with those of PP, resulted from the contribution of well-dispersed MMT sheets.

Generally, increasing the clay content in polymer composites will induce greater increases in G' and η^* at low frequencies.[17,19] Also, greater increases in G' and η^* can result from a better dispersion of the clay in the polymer.[20,21] These two nanocomposites had the same amount of organoclay. The dispersion of modified MMTs in PP3 and PP5 was characterized with WAXD and TEM. As shown in Figure 6, the (001) diffraction peak of PP5 was located at a

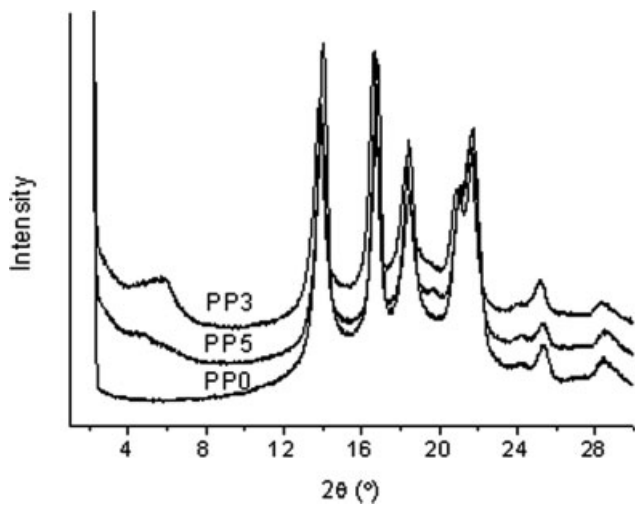

Figure 6 WAXD patterns of PP0, PP5, and PP3.

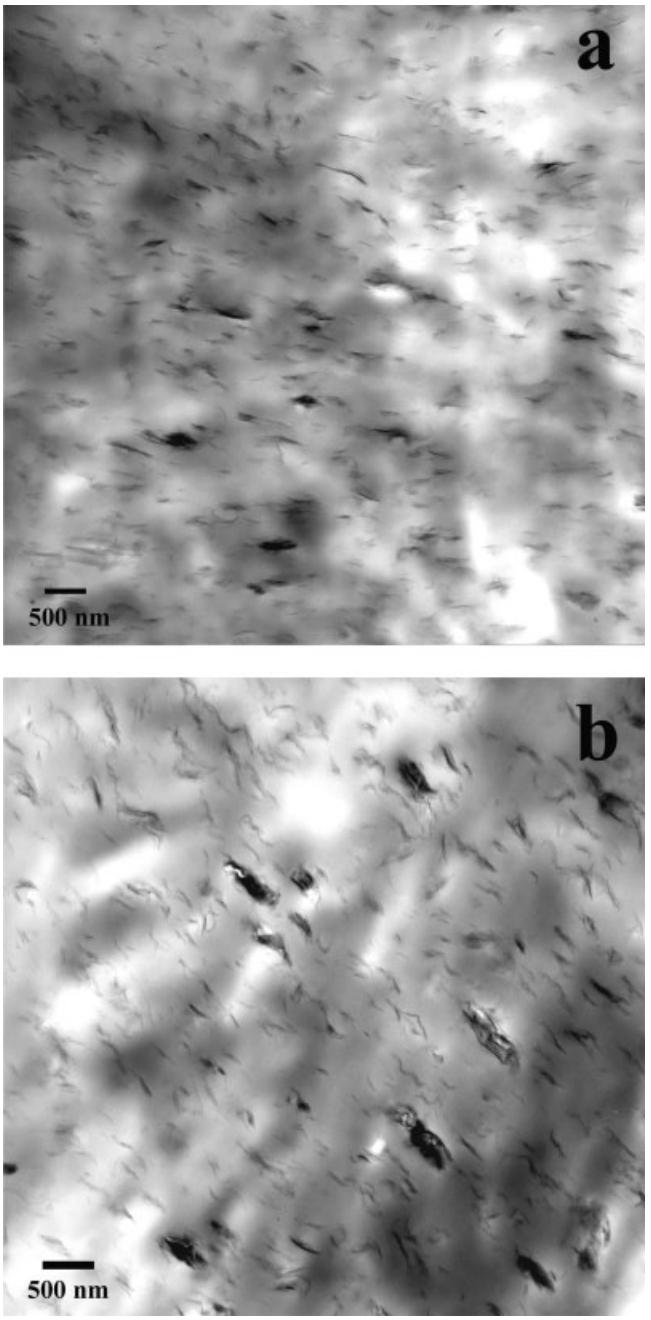

Figure 7 TEM images of (a) PP5 and (b) PP3.

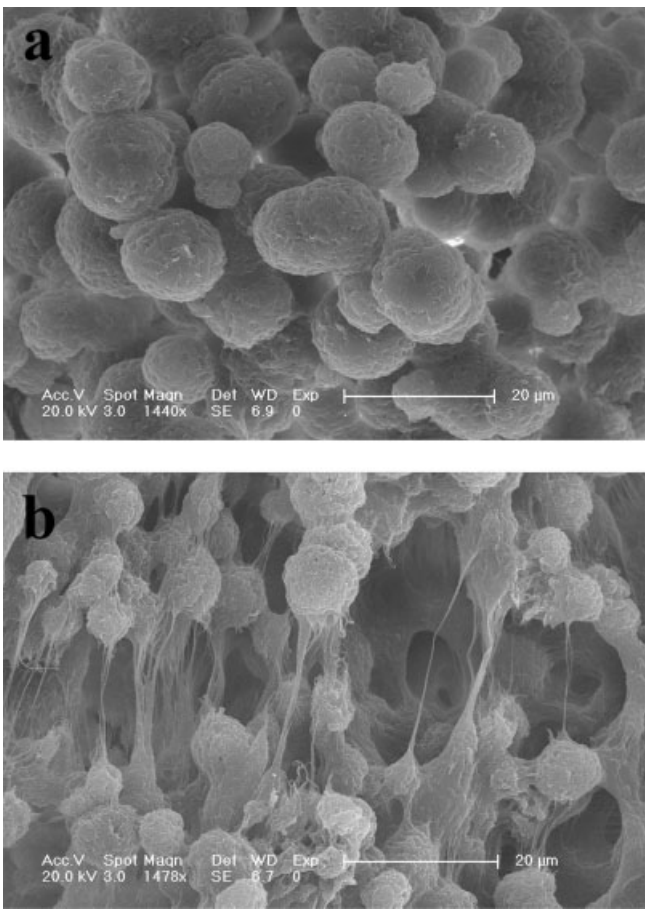

Figure 8 Scanning electron microscopy images of the residue of (a) PP5 and (b) PP3 after Soxhlet extraction.

lower angle with a larger *d*-spacing, and its intensity was lower, in comparison with that of PP3. This means that the dispersion of the F-organoclay in PP3 was not better than that of the CTAB-modified MMT in PP5. This is also confirmed by TEM images in Figure 7. The clay tactoid, composed of several MMT layers, was well dispersed in PP5. PP5 had an intercalated structure. However, large clay aggregates were also observed in PP3, except for the well-dispersed clay tactoid. Thus, there must be another reason for the greater increase in G' and η^* at low frequencies in PP3.

When PP was reactively extruded with a multifunctional monomer, branched, physically connected, and crosslinked architectures were introduced, and this resulted in improvements in G' and η^* of PP at low frequencies.[13,22] The F-organoclay with bonded C=C groups could be used as a multifunctional monomer. In the melt-blending process, PP underwent β scission, and then the resultant fragmental free radical reacted with C=C groups of the F-organoclay and covalently grafted to MMT sheets. The greater increase in G' and η^* of PP3 mainly came from a long-chain-branched and physically connected structure and even a crosslinked architecture in the system. It is speculated that the interfacial interaction was improved between the PP and F-organoclay.

Extraction experiments were used to investigate the interfacial interaction in the PP nanocomposites. Figure 8 shows the morphologies of the residue after extraction. The residue of PP5 was composed of MMT aggregates because the PP matrix was extracted with boiling xylene. However, the residue of PP3 contained a small amount of PP and MMT aggregates. It is evident that MMT aggregates were linked by some PP, as shown in Figure 8(b). As is known, boiling xylene extracts only free PP chains. It was confirmed that some of the PP chains were grafted to MMT layers in PP3 because of the introduction of C=C groups into MMT sheets, so the interfacial interaction was improved between the PP and organoclay. Very interestingly, MMT sheets aggregated together to form a microspherical structure, and the average size of the MMT aggregates in PP3 was smaller than that in PP5. It is possible that self-assembly of MMT sheets takes place during

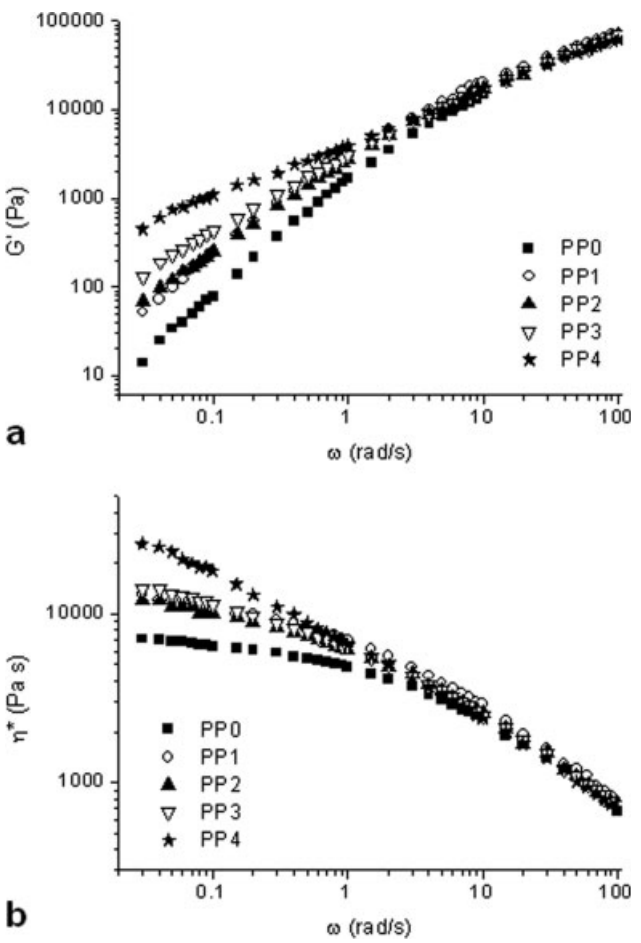

Figure 9 (a) G' and (b) η^* as functions of the angular frequency (ω) for PP composites with different contents of F-organoclay.

TABLE II
Mechanical Properties of the PP Nanocomposites

Sample	Tensile strength (MPa)	Elongation at break (%)	Young's modulus (MPa)
PP0	40.3 ± 0.9	17.0 ± 3.0	864 ± 79
PP1	40.2 ± 0.6	15.0 ± 1.5	911 ± 80
PP2	40.1 ± 0.8	13.0 ± 4.0	1002 ± 68
PP3	40.6 ± 0.4	8.9 ± 1.2	1123 ± 43
PP4	33.5 ± 1.6	4.0 ± 1.1	1106 ± 113
PP5	38.6 ± 0.6	10.0 ± 1.0	844 ± 63
PP6	39.6 ± 0.4	17.9 ± 0.6	765 ± 60

extraction, and this will be explored in further research.

Here, PPMA1001 was used as a compatibilizer to improve the dispersion of the organoclay in PP. PPMA1001 first intercalated into the gallery of MMT and then promoted the intercalation of PP chains into these interlayers. Just like PP chains, PPMA1001 could undergo β scission and produce fragmental free radicals, so PPMA1001 also reacted with C=C groups and covalently grafted to the edge of MMT sheets. The (001) diffraction peak in PP3 (Fig. 6) shifted to a higher angle in comparison with that of the F-organoclay, and this might be related to the improved interfacial interaction. After a polymer chain was grafted to MMT sheets, shear stress made the polymer matrix move during melt processing, so some of the MMT sheets were drawn out and rearranged.

Figure 9 shows plots of G' and η^* as functions of the angular frequency for PP nanocomposites with different contents of the F-organoclay. G' and η^* of the PP nanocomposites increased gradually with the content of the F-organoclay in the low frequency region. This was ascribed to the higher content of the F-organoclay and more C=C groups used, which could increase the crosslinked points and the interfacial interaction between PP and MMT sheets.

Mechanical properties of the PP/F-organoclay nanocomposites

The tensile mechanical properties of the PP nanocomposites are summarized in Table II. PP6 (PP/PPMA1001 blend) showed a lower Young's modulus in comparison with pure PP. The tensile strength and elongation at break did not change significantly. This was because PPMA1001 exhibited inferior mechanical properties in comparison with PP on account of its much lower molecular weight. Compared to PP6, PP5 showed a lower tensile strength and elongation at break and a higher Young's modulus. Thus, the addition of the CTAB-modified MMT decreased the tensile strength and elongation at break of the PP nanocomposite. However, for PP3, the addition of the F-organoclay (bearing C=C groups) with the same content evidently increased the Young's modulus and tensile strength and decreased the elongation at break. This was mainly attributed to the improved interfacial interaction between PP and MMT sheets. In all PP nanocomposites containing the F-organoclay, Young's modulus increased in comparison with that of PP, and the elongation at break decreased gradually with the content of the F-organoclay. Meanwhile, the tensile strength remained constant until the content of the F-organoclay was too high. PP4 with 8 wt % F-organoclay displayed a lower tensile strength, which might have been due to the higher concentration of PPMA1001. PPMA1001 exhibited mechanical properties inferior to those of PP, so the excessive addition of PPMA1001 resulted in a deterioration of the mechanical properties of the final nanocomposite.

CONCLUSIONS

A novel F-organoclay bearing C=C groups was successfully synthesized. Compared to the CTAB-modified MMT, the F-organoclay provided PP nanocomposites with higher G' and η^* values at low frequencies. This phenomenon resulted from the strong interfacial interaction between the PP and MMT sheets of the F-organoclay. In melt processing, fragmental free radicals that originated from the degradation of PP chains could react with C=C groups on the edge of MMT sheets. Thus, some of the PP chains were *in situ* grafted to MMT sheets of the F-organoclay, and the interfacial interaction was enhanced. As a result, PP nanocomposites containing the F-organoclay showed better mechanical properties than those blended with the CTAB-modified MMT. Further research is necessary to optimize the synthetic route of the F-organoclay and the preparation method of PP/F-organoclay nanocomposites to realize the potential of the F-organoclay in improving the performances of polymer nanocomposites.

References

1. Alexandre, M.; Dubois, P. Mater Sci Eng R 2000, 28, 1.
2. Ray, S. S.; Okamoto, M. Prog Polym Sci 2003, 28, 1539.
3. Paul, D. R.; Robeson, L. M. Polymer 2008, 49, 3187.

4. Balazs, A. C.; Emrick, T.; Russell, T. P. Science 2006, 314, 1107.
5. Manitiu, M.; Bellair, R. J.; Horsch, S.; Gulari, E.; Kannan, R. M. Macromolecules 2008, 41, 8038.
6. Wang, C. H.; Auad, M. L.; Marcovich, N. E.; Nutt, S. J Appl Polym Sci 2008, 109, 2562.
7. Bourlinos, A. B.; Jiang, D. D.; Giannelis, E. P. Chem Mater 2004, 16, 2404.
8. Wheeler, P. A.; Wang, J.; Baker, J.; Mathias, L. J. Chem Mater 2005, 17, 3012.
9. Shen, W.; He, H. P.; Zhu, J. X.; Yuan, P.; Frost, R. L. J Colloid Interface Sci 2007, 313, 268.
10. Wheeler, P. A.; Wang, J.; Mathias, L. J. Chem Mater 2006, 18, 3937.
11. Wang, X. C.; Tzoganakis, C.; Rempel, G. L. J Appl Polym Sci 1996, 61, 1395.
12. Tsenoglou, C. J.; Gotsis, A. D. Macromolecules 2001, 34, 4685.
13. Tian, J. H.; Yu, W.; Zhou, C. X. Polymer 2006, 47, 7962.
14. Zhao, Z. F.; Tang, T.; Qin, Y. X.; Huang, B. T. Langmuir 2003, 19, 9260.
15. Wan, C. Y.; Bao, X. J.; Zhao, F.; Kandasubramanian, B.; Duggan, M. P. J Appl Polym Sci 2008, 110, 550.
16. Solomon, M. J.; Almusallam, A. S.; Seefeldt, K. F.; Somwangthanaroj, A.; Varadan, P. Macromolecules 2001, 34, 1864.
17. Gu, S. Y.; Ren, J.; Wang, Q. F. J Appl Polym Sci 2004, 91, 2427.
18. Lertwimolnun, W.; Vergnes, B. Polymer 2005, 46, 3462.
19. Wang, K.; Liang, S.; Deng, J. N.; Yang, H.; Zhang, Q.; Fu, Q.; Dong, X.; Wang, D. J.; Han, C. C. Polymer 2006, 47, 7131.
20. Pluta, M. J Polym Sci Part B: Polym Phys 2006, 44, 3392.
21. Ma, H. Y.; Tong, L. F.; Xu, Z. B.; Fang, Z. P. Polym Degrad Stab 2007, 92, 1439.
22. Nam, G. J.; Yoo, J. H.; Lee, J. W. J Appl Polym Sci 2005, 96, 1793.